CHINESE OPTICS LETTERS

Vol. 19, No. 5 | May 2021

Optimizing illumination's complex coherence state for overcoming Rayleigh's resolution limit

Chunhao Liang (梁春豪)[1], Yashar E. Monfared[2], Xin Liu (刘 欣)[1], Baoxin Qi (齐宝鑫)[1], Fei Wang (王 飞)[3*], Olga Korotkova[4**], and Yangjian Cai (蔡阳健)[1,3***]

[1] Shandong Provincial Engineering and Technical Center of Light Manipulations & Shandong Provincial Key Laboratory of Optics and Photonic Device, School of Physics and Electronics, Shandong Normal University, Jinan 250014, China

[2] Department of Chemistry, Dalhousie University, Halifax, NS B3H 4R2, Canada

[3] School of Physical Science and Technology & Collaborative Innovation Center of Suzhou Nano Science and Technology, Soochow University, Suzhou 215006, China

[4] Department of Physics, University of Miami, Coral Gables, Florida 33146, USA

*Corresponding author: fwang@suda.edu.cn

**Corresponding author: o.korotkova@miami.edu

***Corresponding author: yangjiancai@suda.edu.cn

Received July 16, 2020 | Accepted November 8, 2020 | Posted Online February 3, 2021

We suggest tailoring of the illumination's complex degree of coherence for imaging specific two- and three-point objects with resolution far exceeding the Rayleigh limit. We first derive a formula for the image intensity via the pseudo-mode decomposition and the fast Fourier transform valid for any partially coherent illumination (Schell-like, non-uniformly correlated, twisted) and then show how it can be used for numerical image manipulations. Further, for Schell-model sources, we show the improvement of the two- and three-point resolution to 20% and 40% of the classic Rayleigh distance, respectively.

Keywords: optical coherence; imaging; light manipulation.

DOI: 10.3788/COL202119.052601

1. Introduction

Image formation with spatially partially coherent light has been addressed in classic papers and monographs[1–4] in depth but is nevertheless still the subject of acute scientific exploration[5–10]. In the general case of a partially coherent illumination, the formed image cannot be simply expressed as a convolution of the object's transparency and the system's impulse response function, but rather involves four-dimensional (4D) correlation integrals. In order to simplify image computations, several numerical methods have been proposed including coherent-model representation[11], outer-product expansion[12], pupil shift matrix[13], and the elementary-field approach[14]. On the other hand, several somewhat empirical studies showed that the specially modeled complex degree of coherence (CDC) might have a significant impact on the formed image resolution, resulting in overcoming the Rayleigh diffraction limit[15–17]. In particular, it was found in Ref. [15] that the twist phase can lead to an improvement of the two-point image resolution by an order of magnitude, but such a result only applies to axially symmetric points. Through manipulation of the CDC profile, the image resolution was shown to reach about $0.93d_R$ (d_R being the Rayleigh diffraction limit) for a partially correlated azimuthal vortex illumination[16] and about $0.85d_R$ for the Laguerre–Gaussian correlated illumination[17]. Instead of using a certain type of illumination with a fixed CDC class, we propose to construct the optimal realizable CDC. Since the CDC cannot be devised arbitrarily, being a subject of several realizability conditions[18], this makes the studies of the image resolution improvement by adjusting the CDC somewhat complex.

Application of the Bochner's theorem has led to a simple strategy for devising genuine cross-spectral density (CSD) functions[19], hence the CDCs, and has resulted in a "zoo" of novel partially coherent sources[20–26]. Owing to their particular source coherence properties, the radiated beams exhibit a variety of effects on propagation, including self-focusing[20], self-splitting[27], and self-steering[28], and have already found applications in beam shaping, free-space optical communications, and optical trapping[29–31]. Recently, the CDCs with spatially varying phase functions of the Schell type have also been successfully modeled[32] using a simple sliding-function method, which substantially enriched available CDCs for asymmetric

light manipulation[33], including imaging applications. The sources with structured coherence have been synthesized in the laboratory with the help of spatial light modulators (e.g., Refs. [26,29]) and using the van Cittert–Zernike theorem (e.g., Ref. [17]).

In this Letter, we analyze telecentric imaging systems with the most general partially coherent scalar illumination. We first use a pseudo-mode expansion to evaluate the image intensity as a sum of two-dimensional (2D) (not 4D) Fourier integrals. Our new result is not limited to commonly used Schell-like illumination: it is also suitable for non-uniformly correlated[20] or twisted[23] illumination. Then, using this result, we construct the CDC of illumination, in the Schell-model class, for two particular axially symmetric cases: (i) two points and (ii) three points located in the vertices of an equilateral triangle, and analyze possible resolution improvement.

2. Theoretical Analysis

A schematic diagram of the telecentric imaging system is given in Fig. 1. Two lenses, L_1 and L_2 with focal lengths being $f = f_1 = f_2$, constitute a typical $4f$ imaging system with unit image magnification. The object and its image are in the front focal plane of L_1 and the rear focal plane of L_2, respectively.

Let the illumination be radiated by a scalar, stationary source characterized by the CSD function $W_0(\mathbf{r}_1,\mathbf{r}_2,\omega) = \langle E^*(\mathbf{r}_1,\omega) \cdot E(\mathbf{r}_2,\omega)\rangle$, where $\mathbf{r}_1 = (x_1,y_1)$ and $\mathbf{r}_2 = (x_2,y_2)$ are two position vectors in the object plane[18]. Here, E denotes the electric field, where the asterisk and the angle brackets stand for complex conjugate and ensemble average, and ω is the angular frequency (its dependence will be omitted for brevity). With the (complex) object transmittance $O(\mathbf{r})$, the CSD function behind the object becomes

$$W_0'(\mathbf{r}_1,\mathbf{r}_2) = O^*(\mathbf{r}_1)O(\mathbf{r}_2)W_0(\mathbf{r}_1,\mathbf{r}_2). \tag{1}$$

If a coherent impulse response function between the object plane and the image plane is $K(\mathbf{r},\boldsymbol{\rho})$, on the basis of coherence theory, the relation between the CSD functions in the image and the object planes is expressed via the integral

$$W_{\mathrm{im}}(\boldsymbol{\rho}_1,\boldsymbol{\rho}_2) = \int W_0'(\mathbf{r}_1,\mathbf{r}_2)K^*(\mathbf{r}_1,\boldsymbol{\rho}_1)K(\mathbf{r}_2,\boldsymbol{\rho}_2)\mathrm{d}^2\mathbf{r}_1\mathrm{d}^2\mathbf{r}_2, \tag{2}$$

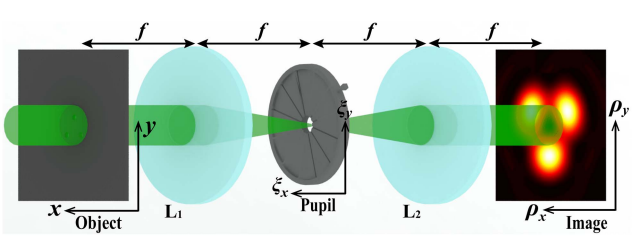

Fig. 1. Schematic diagram for a telecentric imaging system with lenses L_1, L_2 and a pupil.

where $\boldsymbol{\rho}_1$ and $\boldsymbol{\rho}_2$ are the position vectors in the image plane. For the telecentric system with a pupil, the impulse function $K(\mathbf{r},\boldsymbol{\rho})$ is

$$K(\mathbf{r},\boldsymbol{\rho}) = -\frac{1}{\lambda^2 f^2}\int P(\boldsymbol{\xi})\exp\left[-\frac{ik}{f}\boldsymbol{\xi}\cdot(\mathbf{r}+\boldsymbol{\rho})\right]\mathrm{d}^2\boldsymbol{\xi}, \tag{3}$$

where $k = 2\pi/\lambda$ with λ being the wavelength of light, and $P(\boldsymbol{\xi})$ is the complex-valued transmission function of the pupil whose argument may contain the wave aberration of the system. For a genuine CSD of illumination, it suffices to be representable as[19]

$$W_0(\mathbf{r}_1,\mathbf{r}_2) = \tau^*(\mathbf{r}_1)\tau(\mathbf{r}_2)\int p(\mathbf{v})H_0^*(\mathbf{v},\mathbf{r}_1)H_0(\mathbf{v},\mathbf{r}_2)\mathrm{d}^2\mathbf{v}, \tag{4}$$

where $\tau(\mathbf{r})$ is a complex amplitude function, $p(\mathbf{v})$ can be regarded as the power spectral density (hence, must be non-negative), and $\mathbf{v}$ is the 2D position vector in the spatial Fourier plane. For the Schell-model beam, the CDC is the Fourier transform (FT) of the $p(\mathbf{v})$ function, which inspires us to construct the genuine partially coherent beams with any desired CDCs through adopting the suitable $p(\mathbf{v})$ functions. H_0 is an arbitrary kernel. Substitution of Eqs. (1) and (4) into Eq. (2), results in the image-plane spectral density $S_{\mathrm{im}}(\boldsymbol{\rho}) = W_{\mathrm{im}}(\boldsymbol{\rho},\boldsymbol{\rho})$:

$$S_{\mathrm{im}}(\boldsymbol{\rho}) = \int \mathrm{d}^2\mathbf{v}p(\mathbf{v})\left|\int \tau(\mathbf{r})O(\mathbf{r})H_0(\mathbf{v},\mathbf{r})K(\mathbf{r},\boldsymbol{\rho})\mathrm{d}^2\mathbf{r}\right|^2. \tag{5}$$

In Eq. (3), the impulse response function is $K(\mathbf{r},\boldsymbol{\rho}) = K(-\mathbf{r}-\boldsymbol{\rho})$. Therefore, the spectral density in Eq. (5) becomes

$$\begin{aligned} S_{\mathrm{im}}(\boldsymbol{\rho}) &= \int \mathrm{d}^2\mathbf{v}p(\mathbf{v})\left|\int F(\mathbf{v},\mathbf{r})K(-\mathbf{r}-\boldsymbol{\rho})\mathrm{d}^2\mathbf{r}\right|^2 \\ &= \int \mathrm{d}^2\mathbf{v}p(\mathbf{v})|\mathrm{IFT}[\tilde{F}_1(\mathbf{v},\mathbf{f})\tilde{K}(\mathbf{f})]\{-\boldsymbol{\rho}\}|^2, \end{aligned} \tag{6}$$

where $F(\mathbf{v},\mathbf{r}) = \tau(\mathbf{r})O(\mathbf{r})H_0(\mathbf{v},\mathbf{r})$, and the tilde and IFT stand for direct and inverse FT, respectively. It follows from Eq. (6) that the fast FT (FFT) algorithm can be applied to calculate the spectral density in the image plane. First, the integral in the absolute value symbol is evaluated for each $\mathbf{v}$ using the FFT algorithm; then, Eq. (6) is applied to integrate over all values of $\mathbf{v}$. With the help of the pseudo-mode expansion[34], the spectral density $S_{\mathrm{im}}(\boldsymbol{\rho})$ takes an approximate discrete form:

$$S_{\mathrm{im}}(\boldsymbol{\rho}) = \sum_i^N\sum_j^N p(\nu_{xi},\nu_{yj})M(\nu_{xi},\nu_{yj},-\boldsymbol{\rho}), \tag{7}$$

with $M(\nu_{xi},\nu_{yj},-\boldsymbol{\rho}) = |\mathrm{IFT}[\tilde{F}_1(\mathbf{v},\mathbf{f})\tilde{K}(\mathbf{f})]\{-\boldsymbol{\rho}\}|^2$ and $\mathbf{v} = (\nu_{xi},\nu_{yj})$, $(i,j = 1,2,\ldots,N)$. Equations (6) and (7) result in a fast calculation scheme for the image-plane spectral density. In particular, if the source of illumination has circular coherence[35], Eq. (7) could further be reduced to a one-fold summation over $\mathbf{v}$, greatly saving the calculating time. When the illumination is Schell-like, i.e., with the CDC depending on point separation, the spectral density $S_{\mathrm{im}}(\boldsymbol{\rho})$ becomes

$$S_{\mathrm{im}}(\boldsymbol{\rho}) = \int \mathrm{d}^2\mathbf{v}p(\mathbf{v})|\mathrm{IFT}[\tilde{F}_1(\mathbf{f}-\mathbf{v})\tilde{K}(\mathbf{f})]\{-\boldsymbol{\rho}\}|^2, \tag{8}$$

where $F_1(\mathbf{r}) = \tau(\mathbf{r})O(\mathbf{r})$, and $\tau(\mathbf{r})$ is a complex amplitude function. For Schell-model sources, the kernel function in Eq. (4) has the form $H_0(\mathbf{v},\mathbf{r}) = \exp(2\pi i\mathbf{v}\cdot\mathbf{r})$. The result in Eq. (8) is the same as in Ref. [9].

3. Numerical Results

We will now use Eq. (8) to analyze the effect of the CDC on the image resolution under the Schell-model illumination whose CDC only depends on the difference between two position vectors. The Schell-model beams are readily experimentally generated and controlled[18]. Hence, the results derived latter will be more instructive. In the following examples, the illumination's CDC could be optimized based on the coherent imaging theory, where the optimal imaging for the two-point object and the three-point object can be achieved by the phase difference between the adjacent points being π and 2π/3, respectively.

First, let the object be two pinholes located on the x axis, symmetrical with respect to $y = 0$, set at separation d. Then, the object transmission

$$O(\mathbf{r}) = \delta(x - d/2,y) + \delta(x + d/2,y) \tag{9}$$

is a pair of the Dirac-delta functions $\delta(\cdot)$. On substituting Eq. (9) into Eq. (8) and setting $\tau(\mathbf{r}) = \exp(-\mathbf{r}^2/4\sigma_0^2)$, where σ_0 is the beam rms width, we obtain the expression for the image spectral density:

$$S_{\mathrm{im}}(\boldsymbol{\rho}) = \exp(-d^2/8\sigma_0^2)\int \mathrm{d}^2\mathbf{v}\times p(\mathbf{v})\{|S_+|^2 + |S_-|^2 + 2\,\mathrm{Re}[S_+S_-^*\mu(d,0)]\}, \tag{10}$$

where $S_\pm = \tilde{P}(\rho_x \pm d/2,\rho_y)$, $\tilde{P}(\boldsymbol{\rho})$ is the FT of pupil $P(\mathbf{u})$ with $\mathbf{u} = \boldsymbol{\xi}/\lambda f$, and $\mu(\Delta x,\Delta y)$ is the CDC. With $\Delta\mathbf{r} = \mathbf{r}_2 - \mathbf{r}_1 = (\Delta x,\Delta y)$, relation

$$\mu(\Delta\mathbf{r}) = \frac{W(\mathbf{r}_1,\mathbf{r}_2)}{\sqrt{W(\mathbf{r}_1,\mathbf{r}_1)W(\mathbf{r}_2,\mathbf{r}_2)}} = \frac{\int \mathrm{d}^2\mathbf{v}p(\mathbf{v})\exp(2\pi i\mathbf{v}\cdot\Delta\mathbf{r})}{\int \mathrm{d}^2\mathbf{v}p(\mathbf{v})} \tag{11}$$

was used in derivation of Eq. (10) (only valid for Schell-model sources).

Equation (10) is routinely used for the two-pinhole resolution analysis under Schell-model illumination. We assume that the system is aberration-free, i.e., $P(\boldsymbol{\xi}) = |P(\boldsymbol{\xi})|$, being a hard circular aperture of radius R. Hence,

$$S_\pm = \frac{2\pi R^2}{\lambda^2 f^2}\frac{J_1\left[2\pi R\sqrt{(\rho_x \pm d/2)^2 + \rho_y^2}/\lambda f\right]}{2\pi R\sqrt{(\rho_x \pm d/2)^2 + \rho_y^2}/\lambda f}, \tag{12}$$

where J_1 is the Bessel function of the first kind and order one. Since in Eq. (10) $S_\pm$ are real functions, $S_+S_-^* = S_+S_-$. This result is consistent with that reported in Ref. [17]. When illumination is incoherent, $\mu(d,0) = 0$, the minimum resolvable separation (MRS) of two pinholes is given by the well-known Rayleigh criterion: $d_R = 0.61\lambda f/R$. The Rayleigh criterion states that the MRS is met if the position of the first zero of one pinhole image coincides with the position of the maximum point of the other pinhole image. However, the resolution will exceed the Rayleigh limit if the real part of the CDC at $(d,0)$ has a negative value (the closer the CDC to −1, the higher the resolution). Nevertheless, owing to the non-negative definiteness of $p(\mathbf{v})$, the CDC cannot be set arbitrarily. It is one of the primary factors limiting the performance of partially coherent illumination in imaging systems. In fact, the minimum value of $\mathrm{Re}[\mu(d,0)]$ is about −0.3 for Laguerre–Gaussian correlated illumination of order six[17]. In order to make $\mathrm{Re}[\mu(d,0)]$ approach −1 (theoretical minimum value), we choose $p(\mathbf{v})$ as

$$p(\mathbf{v}) = e^{-a^2[(\mathbf{v}_x - b/2)^2 + v_y^2]} + e^{-a^2[(v_x + b/2)^2 + v_y^2]}, \tag{13}$$

with real a and b. Substituting Eq. (13) into Eq. (11) yields

$$\mu(\Delta\mathbf{r}) = e^{-\pi^2\Delta r^2/a^2}\cos(\pi\Delta x/b), \tag{14}$$

i.e., being a cosine function with period $2b$ enveloped by a Gaussian function of width a/π.

Figure 2 illustrates the CDC as a function of $\Delta x/b$ at the cross line $\Delta y = 0$ for several values of a/b. For the bigger value of a/b, it implies that we can get a slower envelope function and faster modulation functions of the source CDC, namely the CDC will get a value closer to −1. For $a/b = 15$, the CDC minimum value is about −0.957, which is very close to the theoretical minimum value of −1. From Eq. (14), one may deduce the position of the minimum value by finding $\mathrm{d}\mu(\Delta x,0)/\mathrm{d}\Delta x = 0$, which is $\sin\theta + 2(b/a)^2\theta\cos\theta = 0$, where $\theta = \pi\Delta x/b$. Hence, if ratio a/b is sufficiently large, the position difference Δx, where

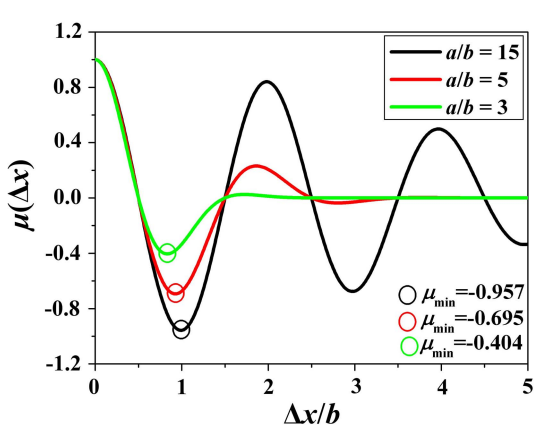

Fig. 2. Variation of CDC with $\Delta x/b$ for different values of a/b.

$\mu(\Delta x,0)$ reaches the minimum value, i.e., the closest to zero solution, is about $\Delta x \approx b$ ($\theta \approx \pi$). Hence, the image of two pinholes reaches appreciable resolution if $b = d$ (distance between two points) for large enough a/b.

Figures 3(a)–3(c) illustrate the density plots of the normalized spectral density $S_{\mathrm{im}}(\boldsymbol{\rho})/[S_{\mathrm{im}}(\boldsymbol{\rho})]_{\max}$ illuminated by beams with the CDC in Eq. (14) for three values of a/b. The distance between two pinholes is set as $d = d_R$. In the calculation of the CDC function, we set $b = d_R$. For comparison, the image of two pinholes illuminated by an incoherent source is illustrated in Fig. 3(d). As expected, the resolution of the two-pinhole image is gradually improved as the value a/b increases. When $a/b = 15$, one can clearly distinguish the images of two points due to the negative correlation of the illumination at the pinholes. The corresponding cross lines of normalized spectral density ($\rho_y = 0$) in Figs. 3(a)–3(d) are shown in Fig. 3(e). Under incoherent illumination, the ratio of the spectral density at $\rho = 0$ to the spectral density maxima is about $S_{\mathrm{im}}(0)/[S_{\mathrm{im}}(\boldsymbol{\rho})]_{\max} = 0.735$, whereas the ratio decreases to 0.0286 when illumination is cosine-Gaussian correlated with $a/b = 15$.

To assess the MRS of two pinholes, we plot in Figs. 4(a)–4(c) their image for three values of $d = b$ at $a/b = 15$. The corresponding cross lines ($\rho_y = 0$) are shown in Fig. 4(d). As separation distance d decreases, the image gradually blurs. When it is about $0.22d_R$, the ratio $S_{\mathrm{im}}(0)/[S_{\mathrm{im}}(\boldsymbol{\rho})]_{\max}$ is just 0.735, reaching the MRS of two pinholes. Figure 4(e) shows the dependence of the MRS of two pinholes on the value of a/b. As expected, the resolution monotonically decreases with the increase of a/b. When $a/b = 20$, the MRS is about $0.18d_R$.

Three pinholes placed at the vertices of an equilateral triangle with side d can be characterized by transmission function

$$O_1(\mathbf{r}) = \delta(x, y - d/\sqrt{3}) + \delta(x - d/2, y + \sqrt{3}d/6) + \delta(x + d/2, y + \sqrt{3}d/6). \tag{15}$$

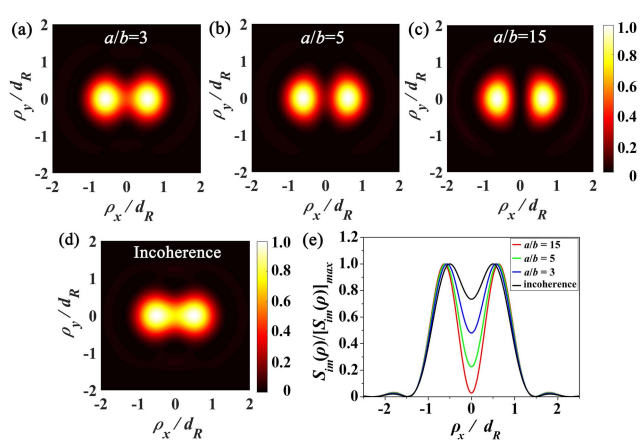

Fig. 3. Images of two pinholes under (a)–(c) partially coherent illumination (normalized S_{im}) for three values of ratio a/b; (d) incoherent illumination; (e) the cross lines ($\rho_y = 0$) of S_{im} in (a)–(d).

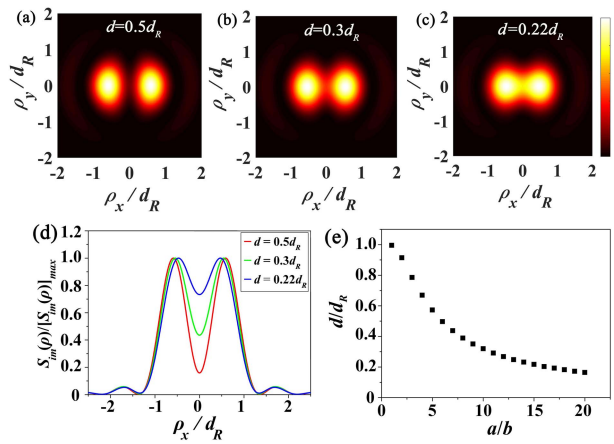

Fig. 4. (a)–(c) Images (S_{im}) of two pinholes with three values of d under partially coherent illumination with $a/b = 15$; (d) cross lines ($\rho_y = 0$) of S_{im} in (a)–(d); (e) dependence of resolution on ratio a/b.

Using Eq. (15) in Eq. (8), we get for the image spectral density

$$S_{\mathrm{im}}(\rho) = \exp\left(-\frac{d^2}{6\sigma^2}\right)\Bigg\{|S_1|^2 + |S_2|^2 + |S_3|^2 + 2\,\mathrm{Re}\Bigg[S_1 S_2^* \times \mu\left(-\frac{d}{2}, \frac{\sqrt{3}d}{2}\right) + S_1^* S_2 \mu\left(-\frac{d}{2}, -\frac{\sqrt{3}d}{2}\right) + S_2 S_3^* \mu(d,0)\Bigg]\Bigg\}, \tag{16}$$

where $S_1 = \tilde{P}(\rho_x, \rho_y + \frac{d}{\sqrt{3}})$, $S_2 = \tilde{P}(\rho_x + \frac{d}{2}, \rho_y - \frac{d}{2\sqrt{3}})$, and $S_3 = \tilde{P}(\rho_x - \frac{d}{2}, \rho_y - \frac{d}{2\sqrt{3}})$. For the best resolution of such an object, the real part of the CDC at $(-d/2, \sqrt{3}d/2)$, $(-d/2, -\sqrt{3}d/2)$, and $(d,0)$ must approach minimum possible (negative) values simultaneously. In order to obtain such a CDC, we set

$$p(\mathbf{v}) = e^{-a^2\left[\left(v_x - \frac{1}{\sqrt{3}b}\right)^2 + v_y^2\right]} + e^{-a^2\left[\left(v_x + \frac{1}{2\sqrt{3}b}\right)^2 + \left(v_y + \frac{1}{2b}\right)^2\right]} + e^{-a^2\left[\left(v_x + \frac{1}{2\sqrt{3}b}\right)^2 + \left(v_y - \frac{1}{2b}\right)^2\right]}. \tag{17}$$

Substituting Eq. (17) into Eq. (11) results in the CDC in form

$$\mu(\Delta\mathbf{r}) = \frac{1}{3} e^{-\frac{\pi^2 \Delta r^2}{a^2}} \left[2\cos\left(\frac{\pi \Delta y}{b}\right) e^{-\frac{i\pi\Delta x}{\sqrt{3}b}} + e^{i\frac{2\pi\Delta x}{\sqrt{3}b}}\right], \tag{18}$$

which is genuinely complex-valued.

Figure 5 shows variation of its real part with $(\Delta x/b, \Delta y/b)$ for $a/b = 20$ and the corresponding cross line at $\Delta y/b = 0$. In Fig. 5(a), there are six minimum regions located on the vertices of a regular hexagon. Three of them (denoted by white circles) are the sought minimum points. Figure 5(b) shows that the position of the minimum point in the right white circle is (1.15, 0). In fact, it is possible to obtain the positions of minimum points on axis $\Delta y = 0$ by solving equation $\partial \mathrm{Re}[\mu(\Delta\mathbf{r})]/\partial \Delta x|_{\Delta y = 0} = 0$. When a/b is sufficiently large, the solution of this equation

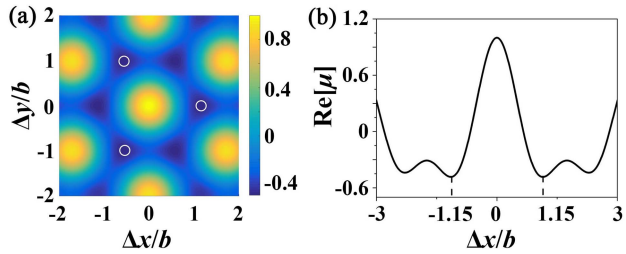

Fig. 5. (a) Density plot of the CDC's real part; (b) cross line ($\rho_y = 0$) at $\Delta y/b = 0$.

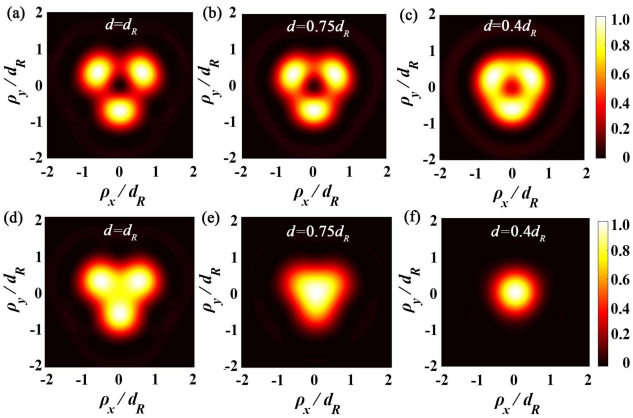

Fig. 6. (a)–(c) Images (S_{im}) of three pinholes with different separations under the illumination of partially coherent beams with the CDC in Eq. (18). (d)–(f) The corresponding images of three pinholes with incoherent illumination.

is $\Delta x = \pm 2\sqrt{3}b/3$. Hence, if $b = \sqrt{3}d/2$, the values of $\mu(-d/2, \sqrt{3}d/2)$, $\mu(-d/2, -\sqrt{3}d/2)$, and $\mu(d,0)$ are about -0.493, i.e., they approach the limiting value of -0.5 as $a/b \to \infty$.

Figures 6(a)–6(c) give the normalized spectral density of a three-pinhole image at three separation values for $b = \sqrt{3}d/2$ and $a/b = 20$. The corresponding images formed with incoherent light are shown in Figs. 6(d)–6(f). When $d = d_R$, the three pinholes are clearly seen with illumination having CDC, as in Eq. (18), whereas they are barely distinguishable with incoherent light. As d decreases, the image gradually blurs. One can still barely distinguish three pinholes at $d = 0.4d_R$ with partially coherent light; while for incoherent light, the image degenerates to a single bright spot [see Fig. 6(f)].

4. Conclusion

In summary, we analyzed imaging with partially coherent illumination by deriving the integral formula involving the shape $p(\mathbf{v})$ function and correlation class $H(\mathbf{r},\mathbf{v})$ on the basis of the pesudo-mode expansion and FFT algorithm. By applying this formula to Schell-like light with predesigned CDC, we found that the image resolution of two pinholes can reach a value as low as $0.18d_R$. In this case, the minimum negative value of the designed CDC is ≈ -0.97, being very close to the ideal minimum value of -1. In the three-pinhole scenario, the resolution of about $0.4d_R$ is achieved for each two-point pair. As compared with the previous work, in which we had improved the image resolution using the Laguerre–Gaussian correlated illumination (the image resolution reached only $0.85d_R$)[17], the current work has demonstrated that one can substantially improve the image resolution of a given object through the optimization design of the illumination's coherence state. Here, we provide our suggestion for experimental realization of a specific Schell-model illumination. As suggested by Ref. [36], generating a specific Schell-model illumination in our work is actually to generate a $p(\mathbf{v})$ function, where the intensity distribution is denoted on the round ground glass disk in the lab. The beam with any desired intensity distribution could be generated by a hologram loaded on a spatial light modulator. We can flexibly adjust the intensity distribution if we choose the different holograms. More details could be found in Ref. [36]. We anticipate that the idea of the active illumination that we introduced can be applied in a variety of the currently used conventional imaging systems, including microscopy and diffraction tomography, and it may generally stimulate the understanding and advancement of optical image formation mechanisms.

Acknowledgement

This work was supported by the National Key Research and Development Program of China (No. 2019YFA0705000), the National Natural Science Foundation of China (Nos. 11525418, 11874046, 11947239, 11974218, and 91750201), the Innovation Group of Jinan (No. 2018GXRC010), and the China Postdoctoral Science Foundation (No. 2019M662424).

References

1. J. W. Goodman, *Statistical Optics* (Wiley, 2000).
2. F. Rojak, "Two-point resolution with partially coherent light," Ph. D. Thesis (Lowell Technological Institute, 1961).
3. D. N. Grimes and B. J. Thompson, "Two-point resolution with partially coherent light," J. Opt. Soc. Am. **57**, 1330 (1967).
4. B. J. Thompson, "Image formation with partially coherent light," Prog. Opt. **7**, 169 (1969).
5. J. Garcia-Sucerquia and R. Castaneda, "Spatial partially coherent imaging," J. Mod. Opt. **49**, 2093 (2002).
6. R. Castaneda, "Phase space representation of spatially coherent imaging," Appl. Opt. **47**, E53 (2008).
7. T. Nakamura and C. Chang, "Exact space invariant illumination for partially coherent imaging systems," J. Opt. Soc. Am. A **27**, 1953 (2010).
8. K. Yamazoe, "Two models for partially coherent imaging," Opt. Lett. **29**, 2591 (2012).
9. K. Yamazoe, "Coherency matrix formulation for partially coherent imaging to evaluate the degree of coherence for image," J. Opt. Soc. Am. A **29**, 1529 (2012).
10. S. A. Ponomarenko, "Self-imaging of partially coherent light in graded-index media," Opt. Lett. **40**, 566 (2015).
11. A. S. Ostrovsky, O. Ramos-Romero, and M. V. Rodriguez-Solfs, "Coherent-mode representation of partially coherent imagery," Opt. Rev. **3**, 492 (1996).
12. J. van der Gracht, "Simulation of partially coherent imaging by outer-product expansion," Appl. Opt. **33**, 3725 (1994).

13. K. Yamazoe, "Computation theory of partially coherent imaging by stacked pupil shift matrix," J. Opt. Soc. Am. A **25**, 3111 (2008).
14. M. Singh, H. Lajunen, J. Tervo, and J. Turunen, "Imaging with partially coherent light: elementary-field approach," Opt. Express **23**, 28132 (2015).
15. Z. Tong and O. Korotkova, "Beyond the classical Rayleigh limit with twisted light," Opt. Lett. **37**, 2595 (2012).
16. D. P. Brown and T. G. Brown, "Partially correlated azimuthal vortex illumination: coherence and correlation measurements and effects in imaging," Opt. Express **16**, 20418 (2008).
17. C. Liang, G. Wu, F. Wang, W. Li, Y. Cai, and S. A. Ponomarenko, "Overcoming the classical Rayleigh diffraction limit by controlling two-point correlations of partially coherent light sources," Opt. Express **25**, 28352 (2017).
18. O. Korotkova, *Random Beams: Theory and Applications* (CRC Press, 2013).
19. F. Gori and M. Santarsiero, "Devising genuine spatial correlation functions," Opt. Lett. **32**, 3531 (2007).
20. H. Lajunen and T. Saastamoinen, "Propagation characteristics of partially coherent beams with spatially varying correlations," Opt. Lett. **36**, 4104 (2011).
21. S. Sahin and O. Korotkova, "Light sources generating far fields with tunable flat profiles," Opt. Lett. **37**, 2970 (2012).
22. L. Ma and S. A. Ponomarenko, "Optical coherence gratings and lattices," Opt. Lett. **39**, 6656 (2014).
23. Z. Mei and O. Korotkova, "Random sources for rotating spectral densities," Opt. Lett. **42**, 255 (2017).
24. M. W. Hyde, "Partially coherent sources generated from the incoherent sum of fields containing random-width Bessel function," Opt. Lett. **44**, 1603 (2019).
25. Z. Mei, "Hyperbolic sine-correlated beams," Opt. Express **27**, 7491 (2019).
26. M. Hyde, IV, S. Bose-Pillai, D. G. Voelz, and X. Xiao, "Generation of vector partially coherent optical sources using phase-only spatial light modulators," Phys. Rev. Appl. **6**, 064030 (2016).
27. Y. Chen, J. Gu, F. Wang, and Y. Cai, "Self-splitting properties of a Hermite–Gaussian correlated Schell-model beam," Phys. Rev. A **91**, 013823 (2015).
28. Y. Chen, S. A. Ponomarenko, and Y. Cai, "Self-steering partially coherent beams," Sci. Rep. **7**, 39957 (2017).
29. S. Avramov-Zamurovic, C. Nelson, S. Guth, and O. Korotkova, "Flat-ness parameter influence on scintillation reduction for multi-Gaussian Schell-model beams propagating in turbulent air," Appl. Opt. **55**, 3442 (2016).
30. Y. Zhou, H. Xu, Y. Yuan, J. Peng, J. Qu, and W. Huang, "Trapping two types of particles using a Laguerre–Gaussian correlated Schell-model beam," IEEE Photon. J. **8**, 6600710 (2016).
31. T. Wu, C. Liang, F. Wang, and Y. Cai, "Shaping the intensity and degree of coherence of a partially coherent beam by a 4*f* optical system with an amplitude filter," J. Opt. **19**, 124010 (2017).
32. O. Korotkova and X. Chen, "Phase structuring of the complex degree of coherence," Opt. Lett. **43**, 4727 (2018).
33. X. Chen and O. Korotkova, "Phase structuring of 2D complex coherence states," Opt. Lett. **44**, 2470 (2019).
34. Y. Gu and G. Gbur, "Scintillation of pseudo-Bessel correlated beams in atmospheric turbulence," J. Opt. Soc. Am. A **27**, 2621 (2010).
35. M. Santrasiero, R. Martinez-Herrero, D. Maluenda, J. C. G. Sande, G. Piquero, and F. Gori, "Partially coherent sources with circular coherence," Opt. Lett. **42**, 1512 (2017).
36. Y. Cai, Y. Chen, and F. Wang, "Generation and propagation of partially coherent beams with nonconventional correlation functions: a review," J. Opt. Soc. Am. A **31**, 2083 (2014).